Spatial Analysis of Metal–PLGA Hybrid Microstructures Using 3D SERS Imaging

Malte S. Strozyk, Dorleta Jimenez de Aberasturi, Jason V. Gregory, Mathias Brust, Joerg Lahann, and Luis M. Liz-Marzán**

The incorporation of gold nanoparticles in biodegradable polymeric nanostructures with controlled shape and size is of interest toward different applications in nanomedicine. Properties of the polymer such as drug loading and antibody functionalization can be combined with the plasmonic properties of gold nanoparticles, to yield advanced hybrid materials. This study presents a new way to synthesize multicompartmental microgels, fibers, or cylinders, with embedded anisotropic gold nanoparticles. Gold nanoparticles dispersed in an organic solvent can be embedded within the poly(lactic-*co*-glycolic acid) (PLGA) matrix of polymeric microstructures, when prepared via electrohydrodynamic co-jetting. Prior functionalization of the plasmonic nanoparticles with Raman active molecules allows for imaging of the nanocomposites by surface-enhanced Raman scattering (SERS) microscopy, thereby revealing nanoparticle distribution and photostability. These exceptionally stable hybrid materials, when used in combination with 3D SERS microscopy, offer new opportunities for bioimaging, in particular when long-term monitoring is required.

1. Introduction

The 21st century is the era of modern nanomedicine, when nanotechnology and biotechnology converge into a new foundation that enables entirely novel modalities for diagnostics, sensing, and therapy.[1,2] The development of new microscopic and spectroscopic techniques combined with the preparation of nanomaterials with a high degree of control is crucial to the development of new drug carrier systems and therapeutic methods.[3] One example is given by surface-enhanced Raman scattering (SERS), a ultrasensitive imaging tool, which, in combination with engineered particle systems, has already found a variety of applications.[4,5] The ability to tune the excitation wavelength into the near infrared (NIR) range, the so-called biological transparency window (650–950 nm), leads to improved light penetration in living tissue, while the low Raman cross section of water and the potential for multiplexed measurements over long periods of time, render this technique ideal for nanomedicine applications.[5–7] For example, Contag, Gambhir, and co-workers recently introduced a Raman spectrometer coupled to an endoscope for SERS-based endoscopy.[8,9] Crucial for this and other applications are nanoparticles functionalized with Raman active molecules (SERS-tags).[5,10] A common strategy toward achieving stable, SERS active nanostructured materials, comprises the integration of both polymers and gold nanoparticles into hybrid materials. Recent examples have been reported for a variety of systems, where, e.g., a thin polymer shell acts as the particle stabilizer, the polymer itself being used as the SERS tag, or where gold particles are embedded in SERS tag-loaded

M. S. Strozyk, Dr. D. Jimenez de Aberasturi, Prof. L. M. Liz-Marzán
CIC biomaGUNE
Paseo de Miramón 182, Donostia-San Sebastián 20014, Spain
E-mail: llizmarzan@cicbiomagune.es
M. S. Strozyk, Prof. M. Brust
Department of Chemistry
University of Liverpool
Liverpool L69 7ZD, UK
Dr. D. Jimenez de Aberasturi, Prof. L. M. Liz-Marzán
CIBER de Bioingeniería, Biomateriales y Nanomedicina
CIBER-BBN
Donostia-San Sebastián 20014, Spain
Dr. J. V. Gregory, Prof. J. Lahann
Biointerfaces Institute Department of Chemical Engineering Materials Science and Engineering
Biomedical Engineering Macromolecular Science and Engineering
B10-A175 NCRC University of Michigan
2800 Plymouth Road, Ann Arbor, MI 48109-2800, USA
E-mail: lahann@umich.edu
Prof. L. M. Liz-Marzán
Ikerbasque
Basque Foundation for Science
Bilbao 48013, Spain

The ORCID identification number(s) for the author(s) of this article can be found under https://doi.org/10.1002/adfm.201701626.

DOI: 10.1002/adfm.201701626

hydrogels.[6,11–13] These systems are often too specific and intrinsically limited to specific shapes, sizes, and surface functionalizations. Embedding metal nanoparticles in a biodegradable polymeric system, which can be modulated in shape and size, would offer more versatile alternatives for applications in nanomedicine. This kind of polymers can be easily used as anchor points for further functionalization with targeting molecules, as cavities for drug loading, or as smart polymers that are responsive to a specific stimulus.[14,15] Interestingly, a simple modification of the size of a polymeric microgel can result in a different cell uptake mechanism.[16] In this context, poly(lactic-*co*-glycolic acid) (PLGA) is a biocompatible (FDA approved)[17] and biodegradable polymer, which is widely used to fabricate nanostructures like microgels, nanoparticles, fibers, or rods.[18,19] PLGA can also be loaded with drugs and functional molecules for further surface functionalization.[20,21] Additional complexity has also been imparted to PLGA nanostructures by implementing multicompartmental structures for highly specific applications, such as drug delivery systems containing two different drugs and distinct release profiles.[22,23] Embedding metal nanoparticles in PLGA particles can be used to combine different optical, electrical, and magnetic features, thereby increasing the range of potential applications.[24] Gold nanoparticles, in contrast to PLGA, are optically active and show interesting behavior upon laser irradiation, including local heating that can be exploited for thermoresponsive delivery methods, as well as the above-mentioned SERS activity, which can be used for imaging.[25] These biological applications are favored for gold nanoparticles with shape anisotropy, such as gold nanostars (AuNSs), which absorb ≈800 nm, where tissue displays reduced absorption and, in turn, increased penetration depth.[26] However, anisotropic nanoparticles are often grown in water or other solvents with high dielectric constants, which may hinder their encapsulation in polymers.[27–29]

We present here a universal method to embed metal nanoparticles of various composition, shape and size, in PLGA nanomaterials by means of the so-called electrohydrodynamic (EHD) co-jetting process. This process has been well established for PLGA over the last decade and offers a high throughput method to synthesize PLGA microgels of different sizes and morphologies.[19] Transfer of gold nanoparticles from water into chloroform ($CHCl_3$)[6,30] was accomplished using hydrophobic SERS active molecules, which act as both capping agents and SERS labels. The resulting nanoparticles with high and reliable SERS signals can be embedded in selected compartments of the PLGA particles, while different fluorescent dyes were added to other compartments, thereby allowing us to expand the standard characterization methods (transmission electron microscopy (TEM), scanning electron microscopy (SEM), and fluorescence microscopy) and using 3D confocal SERS microscopy (3D-SERS) to identify the nanoparticle distribution inside the polymer. To avoid potential interferences arising from the fluorescence of the dyes, these were selected so that their absorption and emission were sufficiently far away from the laser excitation wavelength (785 nm in this case) used for SERS measurements. Even though 3D-SERS imaging offers powerful and complementary possibilities, it is still fairly undeveloped due to its complexity, as the weak nature of the Raman signal and its complicated scattering behavior require finding a suitable compromise for the optimum pinhole size that ensures confocality as well as sufficiently high signal intensity.[31] Recently, a few groups developed substrates to demonstrate Raman imaging with high spatial resolution in 3D.[13,32,33] Especially Ozaki and co-workers recently showed the reconstruction of a 3D plasmonic structure using 3D-SERS.[32] Promising applications for 3D SERS imaging would be, e.g., related to monitoring of implanted scaffolds for tissue regeneration, so as to control their degradation over time, in combination with tissue growth. This is commonly done by using invasive methods such as histology, which do not allow continuous monitoring, while noninvasive methods such as fluorescence microscopy are often limited in penetration depth, sensitivity, and long-term stability, as well as by photobleaching.[34,35]

We introduce here the synthesis of PLGA–metal nanoparticle hybrid materials using EHD co-jetting. AuNSs labeled with different SERS active molecules were embedded in separate compartments of different polymeric structures (particles and fibers), and 3D-SERS imaging was used to monitor the distribution of the particles inside the polymer. We propose that these hybrid materials containing SERS labeled nanoparticles and thus allowing characterization by means of SERS imaging, offer significant advantages over existing fluorescence-based materials for bioimaging.

2. Results and Discussion

2.1. Synthesis of Bicompartmental PLGA Nanoparticles Loaded with SERS Encoded Nanoparticles in Separate Hemispheres

The preparation of hybrid multicompartmental PLGA–plasmonic microparticles is schematically illustrated in **Figure 1**. Nanoparticles synthesized in aqueous solution were transferred into $CHCl_3$ by means of a protocol previously reported by our group.[30] A Raman active molecule was used as surfactant during this process to obtain highly stable and bright SERS tags. The resulting particle suspension was mixed with various amounts of PLGA and different fluorescent dyes: ((Poly[(*m*-phenylenevinylene)-*alt*-(2,5-dihexyloxy-*p*-phenylenevinylene) as a blue dye or poly[tris(2,5-bis(hexyloxy)-1,4-phenylenevinylene)-*alt*-(1,3-phenylenevinylene)] as a green dye.

Gold nanostars were specifically selected for most of the experiments due to their strong absorbance in the NIR range (see TEM images and optical spectra in Figure S1, Supporting Information) and their outstanding performance as SERS tags, to conduct 3D SERS measurements. The Raman active molecules biphenyl-4-thiol (4-BPT) and 2-naphtalene-thiol (2-NAT) were used as ligands due to their strong binding affinity to gold surfaces and their characteristic and easily distinguishable Raman signals. The final particle size was influenced by the solvent composition and the molecular weight of PLGA.[19] When using 17 kDa PLGA and 70:30 $CHCl_3$:DMF, particles of ≈600–800 nm were obtained, whereas 40 kDa PLGA in 70:30 $CHCl_3$:DMF yielded particles of ≈1–2 µm, and using 50–75 kDa PLGA and solvent ratios between 70:30 and 97:3 $CHCl_3$:DMF, particles in the range of 3–8 µm could be produced.

In order to demonstrate universality of the method, we also prepared polymeric particles containing SERS-encoded 30 nm

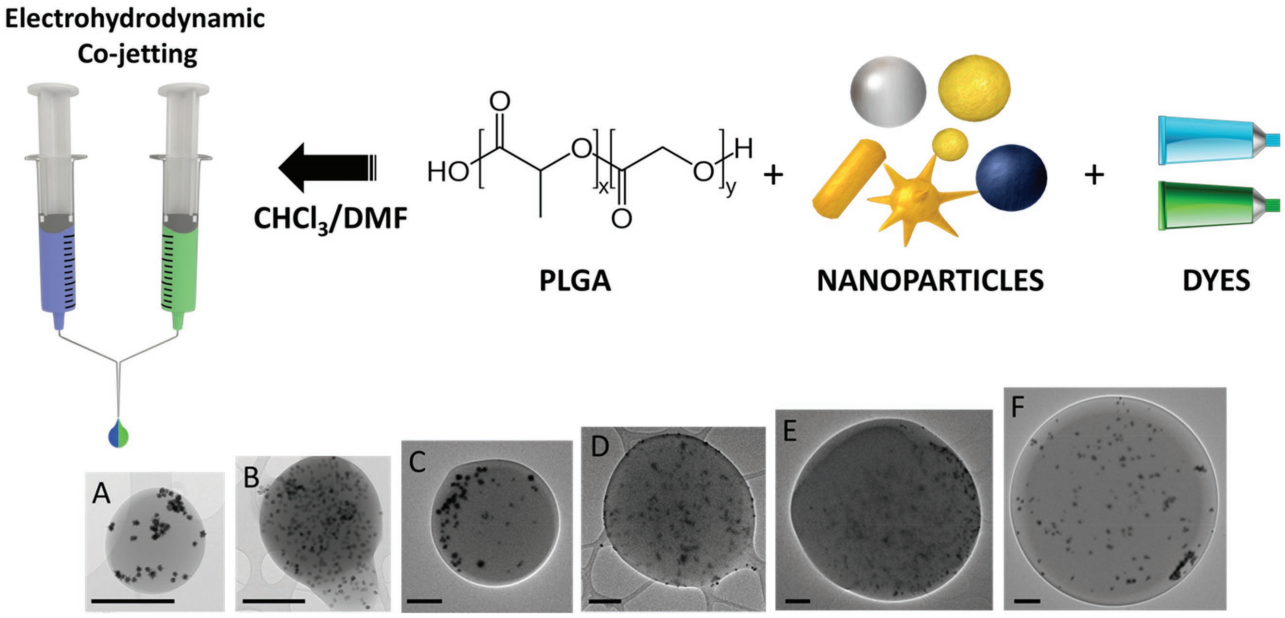

Figure 1. Fabrication of multicompartmental hybrid particles using electrohydrodynamic co-jetting. The size of the particles can be controlled by using different polymer molecular weights and varying polymer concentrations. TEM images in A–F are representative for particles of different sizes and compositions. PLGA molecular weight was varied from A,B) 17 kDA through C,D) 40 kDA up to E,F) 50–75 kDA. These examples show various configurations with two (A, C–F) or three (B) compartments, containing AuNSs (A–F) and iron oxide nanoparticles (B). The particles also contain poly[(*m*-phenylenevinylene)-*alt*-(2,5-dihexyloxy-*p*-phenylenevinylene) as a blue dye and poly[tris(2,5-bis(hexyloxy)-1,4-phenylenevinylene)-alt-(1,3-phenylenevinylene)] as a green dye, in separate compartments. All scale bars are 500 nm.

AgNPs and 40 nm iron oxide particles (Figure 1; Figures S2 and S3, Supporting Information). AgNPs are ideal for SERS measurements at laser excitation wavelengths ≈500–600 nm, whereas magnetic nanoparticles could be used to separate/collect the hybrid particles by magnetophoresis. In an additional experiment, the PLGA surface was functionalized with carboxylic acid groups, by adding 30% of 5050 DLG 1A polymer (5.9 kDa) to the initial PLGA/AuNSs mixture (Figure S4A, Supporting Information). For subsequent experiments, these can be useful as anchor points for further (bio) functionalization, e.g., with antibodies.

For EHD co-jetting, the polymer/particle/dye mixtures were flown in a laminar regime through parallel mounted metallic needles at 0.2 mL per hour. After a stable droplet was formed at the interface of the polymeric solutions, a voltage was applied between the droplet and a collector plate. The voltage created a polymeric jet from the tip of the droplet towards the collector and was sufficiently high to induce break-up of the jet into individual particles. Transmission electron microscopy (TEM), scanning electron microscopy (SEM), and fluorescence microscopy studies demonstrate that particles evenly formed over a large area (Figure S4, Supporting Information).

2.2. Stability of the Compartments

PLGA hybrid microgels showed high particle loading, regardless of the type of plasmonic particles used in the synthesis, as observed in TEM images (Figure 1A–F). However, TEM images alone could not resolve the different compartments within the particles. Therefore, the inner distribution and the preservation of the different compartments after synthesis were characterized by means of fluorescence imaging (from blue and green dyes) and SERS imaging (from two different SERS-encoded AuNSs).

Once synthesized, polymeric particles were embedded in a ProLong™ gold matrix between two coverslips and initially examined by confocal fluorescence microscopy (**Figure 2**A). For SERS measurements, the particles were immobilized on a quartz glass slide to avoid the fluorescence background from standard glass and then examined under a WITec Alpha 300RS confocal Raman microscope, using a 785 nm diode laser as the excitation source. As a reference, we used the Raman bands at 1275 cm^{-1} for 4-BPT (C—C ring stretch) and 1375 cm^{-1} for 2-NAT (C—C ring stretch), so that the characteristic bands of both Raman reporters could be clearly distinguished (**Figure 3**B). In Figure 2B,C, both fluorescence and SERS images indicate the stability and preservation of the two initial compartments. Interestingly, no interference from the fluorescent dyes was observed, and as a result the shape of the compartments was clearly resolved by both techniques. The SERS images also allowed for differentiation of the compartments, but in contrast to fluorescence imaging, the SERS signal was not found to be evenly distributed throughout the entire particle. This is due to the distribution of AuNSs, which, in contrast to the dyes, may associate into clusters within the PLGA compartments, resulting in a distinct pattern with islands of higher intensity in the SERS maps. Figure 2C also shows a dominant signal from 4-BPT in this form of representation and reveals lack of information regarding the inner particle distribution. For this reason, 3D SERS imaging was conducted, focusing on obtaining spatial information in x, y, and z directions.

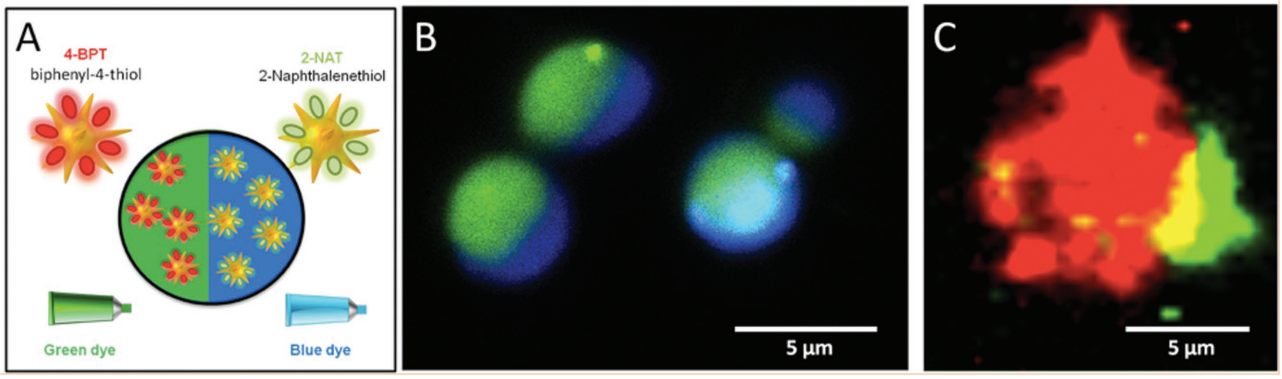

Figure 2. A) Bicompartmental PLGA (40 kDa) particles containing ≈50 nm AuNSs labeled with 4-BPT and a green dye in one compartment, and AuNSs labeled with 2-NAT and a blue dye in the other compartment. B) Fluorescence image of ≈4 µm particles showing that both dyes and compartments are well separated and distinguishable. C) SERS mapping of a ≈7 µm particle, also displaying two separate compartments. The signals from 4-BPT (red) and 2-NAT (green) are spatially separated.

The 3D distribution of SERS-encoded AuNSs inside the microgel particles was examined with high-resolution confocal Raman microscopy. We selected a 100× 0.9 NA objective with a 50 µm pinhole that best met our requirements.[31] One particle was scanned over a volume of $14 \times 14 \times 20$ µm^3 ($40 \times 40 \times 35$ points per line), with an integration time of 40 s per line (785 nm laser, 7 mW). The observed signal-to-noise-ratios were in general very high and the SERS spectra for both Raman tags were well resolved under these scanning conditions (Figure 3B). A series of slices (in z-direction) were imaged, in which both SERS tags (2-NAT, 4-BPT) could be resolved, indicating spatial separation within different compartments. Even though some degree of overlap (yellow–orange color) was observed, the compartments were found to be well separated from each other in most cases. Additional 3D reconstructions (Figure 3C,D) confirm these results and suggest that the compartments are not perfect hemispheres but rather have a "tennis ball" like structure, where both compartments are wrapped around each other. In conclusion, we show that SERS labeled AuNSs are present throughout the microgel and their distribution can be resolved by confocal Raman microscopy. This 3D reconstruction especially helps to achieve information about nanoparticle distribution, which is not possible by conventional SERS measurements.

2.3. Labeled Fibers and Rods

One of the challenges related to monitoring the evolution and degradation of scaffolds during tissue growth is related to a low penetration depth when using fluorescence microscopy (usually with illumination and fluorescence in the visible). Since PLGA electrospun nanofibers have been reported as scaffolds for cell or tissue growth,[36] we explored the possibility to synthesize PLGA fibers containing AuNSs, while preserving

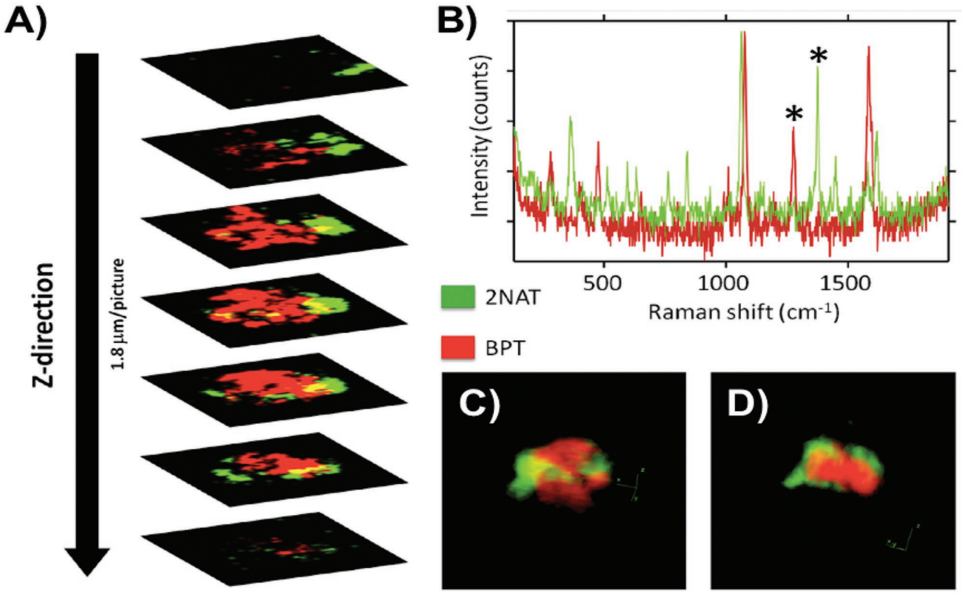

Figure 3. 3D confocal Raman imaging of a single microgel particle. A) Z-stack showing the existence of separated compartments and the distribution of SERS labeled AuNSs within the particle. B) Representative SERS spectra of BPT (red) and 2-NAT (green) labeled AuNSs measured inside PLGA particles. The peaks marked with * indicate the specific signals used for mapping. C,D) 3D reconstruction of the particle from two different perspectives.

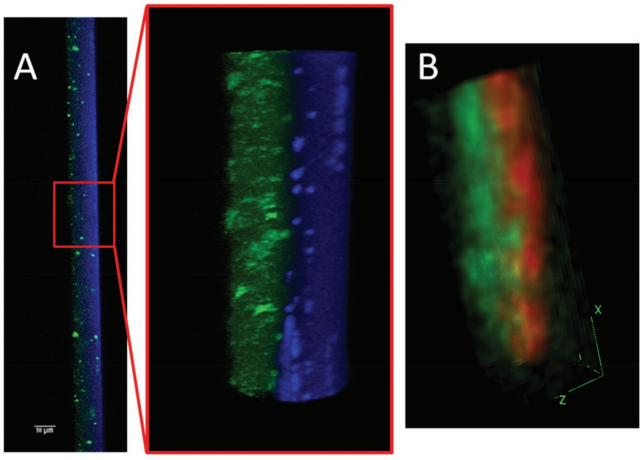

Figure 4. Examples of PLGA-based bicompartmental fibers containing SERS-encoded AuNSs, prepared by electrohydrodynamic co-jetting and analyzed by A) fluorescence imaging and B) SERS mapping.

their bicompartmental structure (**Figure 4**). We thus prepared fibers with a diameter of 10 µm, i.e., twice as large as the particles above, which would likely facilitate the resolution of the different compartments. SERS imaging indeed showed a distinct separation between the compartments filled with 4-BPT-coated AuNSs and 2-NAT-coated AuNSs (Figure 4B). The 3D reconstruction of the SERS data in Figure 4B confirms yet again that SERS is a useful tool to resolve the structure of our hybrid polymeric structures and the internal structure of the different compartments.

To further demonstrate the universal character of our synthesis protocol, the obtained fibers were cut into pieces, to obtain cylinders with different lengths (Figure S5, Supporting Information). Upon embedding the fibers in a Tissue-Plus matrix and using a cryosectioning instrument (see Experimental Section), it was possible to fabricate cylinders while keeping the two compartments stable.[18] Cylinders are of interest since the shape of particles plays an important role in the modulation of cell uptake, as reported elsewhere.[37]

2.4. Fluorescence versus SERS: Long-Term Experiments

Long-term stability is a key advantage of SERS, as compared to fluorescence, and can be exploited in labeled scaffolds or microgels as imaging tools in nanomedicine. During long-term experiments, the particles are exposed to a number of factors that lead to degradation and bleaching of organic molecules. The environments used for both in vitro and in vivo experiments are chemically aggressive, containing redox active molecules, enzymes, highly reactive radicals and pH changes.[38–40] Additionally, exposure to light during microscopy observation often leads to photobleaching of organic dyes.[41]

We analyzed the effect of photobleaching on our hybrid materials by measuring fluorescence and SERS signals from a large number of particles (>100) before (**Figure 5**A) and after (Figure 5B) UV-irradiation for 30 min. Prior to irradiation, the samples displayed fluorescence and SERS signals throughout the whole field of view. In contrast, after irradiation, the fluorescence signal completely vanished, while the SERS signals remained basically unaltered. This experiment clearly illustrates the degradation of the dye over time upon exposure to light, whereas the SERS tags remain stable and active, in a demonstration that SERS is an attractive tool for long-term (bio)imaging experiments.

3. Conclusions

We have introduced a universal method for the synthesis of PLGA microgels of different sizes and shapes, loaded with dyes and metal nanoparticles with distinct electromagnetic properties. These particles offer a wide range of potential applications, in particular for biomedical imaging. Even though we focused here on PLGA (FDA approved polymer), the EHD co-jetting method facilitates the use of various other polymers (and their blends), including a wide range of synthetic polymers (PMMA, PAA, PEI, Dextran) and more recently crosslinked biopolymers such as proteins. We demonstrated that SERS encoded AuNSs, embedded within polymer microgels, can be used to resolve and reconstruct the shape of both particles and fibers. Importantly, co-loaded dyes do not interfere with the SERS signal or create a background, which is likely due to the high and reliable SERS signal originating from AuNSs densely covered with Raman tags. Finally, an important outcome of this study is the demonstration that the SERS signals from embedded AuNS, in contrast to that from fluorescent dyes, are not altered upon exposure to UV illumination, therefore offering the possibility for long-term imaging experiments. Since PLGA is a biocompatible and biodegradable polymer, potential applications of these hybrid materials can be foreseen, for example in combined drug delivery/imaging devices. In particular, microfibers functionalized with AuNSs may allow us to obtain new insights in the role of implanted scaffolds in regenerative medicine.

4. Experimental Section

Materials: Milli-Q water (resistivity 18.2 MΩ cm) was used in all experiments. Hydrogen tetrachloroaurate trihydrate ($HAuCl_4{\cdot}3H_2O$, ≥99.9%), sodium citrate tribasic dihydrate (≥98%), silver nitrate ($AgNO_3$, ≥99%), L-ascorbic acid (AA, ≥99%), O-[2-(3-mercaptopropionylamino) ethyl]-O′—methylpolyethylene glycol (PEG-SH, M_W = 5 000 g mol^{-1}), 2-naphthalenethiol (2-NaT, 99%), biphenyl-4-thiol (4-BPT, 97%), chloroform (≥99.8%), and 50–75 kDa PLGA, were purchased from Sigma-Aldrich. 17 kDa PLGA (#5002a) and 40 kDa PLGA (#5004a) were purchased from Corbion. 5050 DLG 1A polymer (#LX00560-130) was purchased from Lakeshore Biomaterials. ProLong™ gold matrix was purchased from Thermofisher Scientific. Quartz microscope slides were from Electron microscopy (#72250–01). 5 nm AuNPs and 40 nm iron oxide nanoparticles were purchased from Ocean Nanotech LLC. All glassware was washed with aqua regia, rinsed threefold with Milli-Q water and dried, prior to use.

For EHD co-jetting, a syringe pump (Fisher Scientific Inc., USA) and a power supply (DC voltage source, Gamma High Voltage Research, USA) were used.

Synthesis of Gold Nanostars: AuNSs were prepared using a seed-mediated growth method.[42] Adding 5 mL of 34×10^{-3} M citrate solution to 95 mL of boiling 0.5×10^{-3} M $HAuCl_4$ solution under vigorous stirring and then maintaining boiling for 15 min, seed particles were formed. 50 nm AuNSs with an LSPR maximum at 750 nm, were prepared by adding 2.5 mL

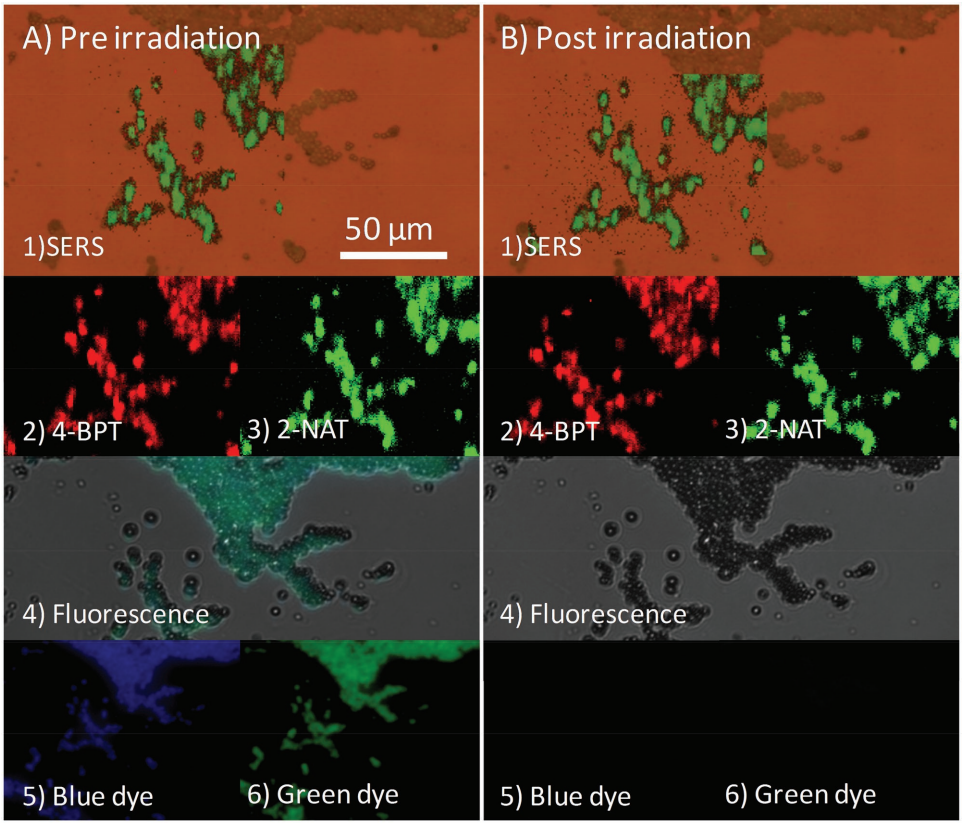

Figure 5. A large number (>100) of bicompartmental particles were immobilized on a glass substrate and both SERS and fluorescence signals were measured A) before and B) after exposure to UV-light. Images 1–3 demonstrate that the SERS signals from both 4-BPT and 2-NAT SERS tags show no difference over time and remain active upon irradiation. The fluorescence signals of both blue and green dyes (4–6) however, vanish after UV light exposure, due to photobleaching of the dye molecules.

of the citrate-stabilized seed solution to 50 mL of 0.25×10^{-3} M $HAuCl_4$ solution (containing 50 µL of 1 M HCl), in a 100 mL glass erlenmeyer at room temperature, under moderate stirring. Quickly, 500 µL of 3×10^{-3} M $AgNO_3$ and 250 µL of 100×10^{-3} M ascorbic acid were added simultaneously. The resulting AuNSs solution was mixed with 410 µL of PEG-SH 0.1×10^{-3} M, stirred for 15 min and washed by centrifugation at 1190 g, 25 min, 10 °C, and subsequently redispersed in water.

Synthesis of Silver Nanoparticles: A modification of a previously reported approach was used to prepare 30 nm Ag NPs.[43] 250 mL of Mili-Q water was heated under magnetic stirring, then 4 mL of trisodium citrate (0.1 M) and 0.32 mL of ascorbic acid (0.1 M) were added to the boiling water. Subsequently, 0.93 mL of $AgNO_3$ (0.1 M) was added and boiling was maintained for 1 h under stirring. The solution was cooled down and stored in the fridge.

Phase Transfer of Plasmonic Nanoparticles: All plasmonic particles were prestabilized with PEG (O-[2-(3-mercaptopropionylamino) ethyl]-O′methylpolyethylene glycol),[6,30] and subsequently transferred from water into $CHCl_3$ by vigorously stirring the colloids with a chloroform solution of the hydrophobic Raman active molecules. Both phases were mixed overnight, so that the particles would slowly diffuse from the aqueous into the organic phase. Afterwards, the aqueous phase was discarded and the organic phase centrifuged several times to remove excess of free ligand.

Bicompartmental PLGA Particles: Bicompartmental PLGA particles were synthesized using 50–75 kDA PLGA (#430471 Aldrich) and a solvent ratio of 97:3 for $CHCl_3$ and DMF. Briefly, in compartment (I) 0.0405 g of PLGA was mixed with 235 µL of green dye (1 mg mL^{-1} in $CHCl_3$) and 485 µL of SERS-Tag (4-BPT) AuNSs [$Au^{\circ} = 3 \times 10^{-3}$ M] in $CHCl_3$ and 15 µL DMF. Compartment (II) was prepared by mixing 0.0405 g of PLGA with 235 µL of blue dye (1 mg mL^{-1} in $CHCl_3$) and 485 µL of SERS-Tag (2-NAT) AuNSs [$Au^{\circ} = 3 \times 10^{-3}$ M] in $CHCl_3$ and 15 µL DMF.

Bicompartmental Fibers: Using a 50–75 kDA PLGA (#430471 Aldrich) and a solvent ratio of 97:3 for $CHCl_3$ and DMF, 10 µm fibers where obtained. In compartment (I) 0.15 g of PLGA was mixed with 54.55 µL of green dye (1 mg mL^{-1} diluted in $CHCl_3$) and 350 µL of SERS-Tag (4-BPT) AuNSs [$Au^{\circ} = 3 \times 10^{-3}$ M] in $CHCl_3$ and 15 µL DMF. Compartment (II) was prepared by mixing 0.15 g of PLGA with 54.55 µL of blue dye (1 mg mL^{-1} in $CHCl_3$) and 350 µL of SERS-Tag (2-NAT) AuNSs [$Au^{\circ} = 3 \times 10^{-3}$ M] in $CHCl_3$ and 15 µL DMF.

Bicompartmental Cylinders: Bicompartmental fibers were deposited in an aligned orientation on a tissue cryomold, and then embedded in a Tissue-Plus matrix. They were stored at −4 °C for 24 h, after being cut using a Leica 3050S cryostat cryosectioning instrument. The obtained slides were collected in falcon tubes and washed several times by centrifugation and redispersion in water. Cylinders of 2, 5, and 10 µm were obtained, as defined by the cutting plane size.

SERS Measurements: SERS measurements (except bleaching experiment) were carried out using a WITec Alpha 300RS micrcoscope with a 100× 0.9 NA objective, a 600 g mm^{-1} diffraction grating and a 785 nm Laser source with a power of about 7 mW.

3D Reconstruction: For each z-height, a single point map was created by plotting the intensity of a selected band for each SERS tag (1275 cm^{-1} for 4BPT and 1375 cm^{-1} for 2-NAT), as a function of the position. The resulting maps were merged using ImageJ and 3D reconstructions were created using the ImageJ plugin 3D Viewer.

Bleaching Experiment: The microgel suspension was dropcast on a quartz glass slide and SERS maps were measured using a Renishaw inVia Raman microscope, equipped with a 1024 × 512 CCD detector, using a

785 nm excitation source and a 1200 g mm^{-1} diffraction grating. Measurements were carried out using a 100× 0.85 NA objective in Streamline mode, with 2.1 mW laser power and an exposure time of 3.58 s. The slide was transferred to a Zeiss Cell Observer microscope, where fluorescence images under 20× magnification were obtained and then the LED diodes were used to illuminate the sample. In general, the samples were illuminated for 30 min with the 470 and 530 nm lasers, with powers of 11.6 and 2.3 mW, respectively. Fluorescence images and SERS measurements were repeated and processed under the exact same conditions.

Supporting Information

Supporting Information is available from the Wiley Online Library or from the author.

Acknowledgements

This work was funded by the European Union's Horizon 2020 Program under the Marie Sklodowska-Curie grant HYMADE, agreement n° 645686.

Conflict of Interest

The authors declare no conflict of interest.

Keywords

3D surface-enhanced Raman scattering imaging, gold nanostars, PLGA particles, SERS tags

Received: March 28, 2017
Revised: May 18, 2017
Published online:

[1] P. D. Howes, R. Chandrawati, M. M. Stevens, *Science* **2014**, *346*, 1247390.
[2] R. Duncan, M. J. Vicent, *Adv. Drug Delivery Rev.* **2013**, *65*, 60.
[3] R. Duncan, R. Gaspar, *Mol. Pharm.* **2011**, *8*, 2101.
[4] E. C. Dreaden, A. M. Alkilany, X. Huang, C. J. Murphy, M. A. El-Sayed, *Chem. Soc. Rev.* **2012**, *41*, 2740.
[5] Y. Wang, S. Kang, J. D. Doerksen, A. K. Glaser, J. T. C. Liu, *IEEE J. Sel. Top. Quantum Electron.* **2016**, *22*, 154.
[6] D. Jimenez de Aberasturi, A. B. Serrano-Montes, J. Langer, M. Henriksen-Lacey, W. J. Parak, L. M. Liz-Marzán, *Chem. Mater.* **2016**, *28*, 6779.
[7] G. McNay, D. Eustace, W. E. Smith, K. Faulds, D. Graham, *Appl. Spectrosc.* **2011**, *65*, 825.
[8] E. Garai, S. Sensarn, C. L. Zavaleta, N. O. Loewke, S. Rogalla, M. J. Mandella, S. A. Felt, S. Friedland, J. T. C. Liu, S. S. Gambhir, C. H. Contag, *PLoS One* **2015**, *10*, e0123185.
[9] C. L. Zavaleta, E. Garai, J. T. C. Liu, S. Sensarn, M. J. Mandella, D. Van de Sompel, S. Friedland, J. Van Dam, C. H. Contag, S. S. Gambhir, *Proc. Natl. Acad. Sci. USA* **2013**, *110*, E2288.
[10] S. Kang, Y. Wang, N. P. Reder, J. T. C. Liu, *PLoS One* **2016**, *11*, e0163473.
[11] G. Bodelón, V. Montes-García, C. Fernández-López, I. Pastoriza-Santos, J. Pérez-Juste, L. M. Liz-Marzán, *Small* **2015**, *11*, 4149.
[12] Y. Wang, B. Yan, L. Chen, *Chem. Rev.* **2013**, *113*, 1391.
[13] Q. Zhang, Y. H. Lee, I. Y. Phang, C. K. Lee, X. Y. Ling, *Small* **2014**, *10*, 2703.
[14] M. R Aguilar, J. San Roman, *Smart Polymers and Their Applications*, Elsevier, Amsterdam, NL **2014**.
[15] M. A. Cohen Stuart, W. T. S. Huck, J. Genzer, M. Müller, C. Ober, M. Stamm, G. B. Sukhorukov, I. Szleifer, V. V. Tsukruk, M. Urban, F. Winnik, S. Zauscher, I. Luzinov, S. Minko, *Nat. Mater.* **2010**, *9*, 101.
[16] T. Sun, Y. S. Zhang, B. Pang, D. C. Hyun, M. Yang, Y. Xia, *Angew. Chem., Int. Ed.* **2014**, *53*, 12320.
[17] http://www.americanpharmaceuticalreview.com/Featured-Articles/188841-FDA-s-Regulatory-Science-Program-for-Generic-PLA-PLGA-Based-Drug-Products/ (accessed: March 2017, *FDA's Regulatory Science Program for Generic PLA/PLGA-Based Drug Products*).
[18] S. Bhaskar, J. Hitt, S.-W. L. Chang, J. Lahann, *Angew. Chem. Int. Ed.* **2009**, *48*, 4589.
[19] S. Rahmani, S. Ashraf, R. Hartmann, A. F. Dishman, M. V. Zyuzin, C. K. J. Yu, W. J. Parak, J. Lahann, *Bioeng. Transl. Med.* **2016**, *1*, 82.
[20] F. Danhier, E. Ansorena, J. M. Silva, R. Coco, A. Le Breton, V. Préat, *J. Controlled Release* **2012**, *161*, 505.
[21] H. K. Makadia, S. J. Siegel, *Polymers* **2011**, *3*, 1377.
[22] S. Rahmani, A. M. Ross, T.-H. Park, H. Durmaz, A. F. Dishman, D. M. Prieskorn, N. Jones, R. A. Altschuler, J. Lahann, *Adv. Healthcare Mater.* **2016**, *5*, 94.
[23] J. Lahann, *Small* **2011**, *7*, 1149.
[24] D. W. Lim, S. Hwang, O. Uzun, F. Stellacci, J. Lahann, *Macromol. Rapid Commun.* **2010**, *31*, 176.
[25] A.-I. Henry, B. Sharma, M. F. Cardinal, D. Kurouski, R. P. Van Duyne, *Anal. Chem.* **2016**, *88*, 6638.
[26] R. Weissleder, *Nat. Biotechnol.* **2001**, *19*, 316.
[27] N. Li, P. Zhao, D. Astruc, *Angew. Chem. Int. Ed.* **2014**, *53*, 1756.
[28] J. Yang, J. Y. Lee, J. Y. Ying, *Chem. Soc. Rev.* **2011**, *40*, 1672.
[29] M. Lista, D. Z. Liu, P. Mulvaney, *Langmuir* **2014**, *30*, 1932.
[30] A. B. Serrano-Montes, D. Jimenez de Aberasturi, J. Langer, J. J. Giner-Casares, L. Scarabelli, A. Herrero, L. M. Liz-Marzán, *Langmuir* **2015**, *31*, 9205.
[31] T. Dieing, O. Hollricher, J. Toporski, *Confocal Raman Microscopy*, Springer Science & Business Media, Berlin, Heidelberg **2011**.
[32] S. Vantasin, W. Ji, Y. Tanaka, Y. Kitahama, M. Wang, K. Wongravee, H. Gatemala, S. Ekgasit, Y. Ozaki, *Angew. Chem. Int. Ed.* **2016**, *55*, 8391.
[33] Q. Jin, M. Li, B. Polat, S. K. Paidi, A. Dai, A. Zhang, J. V. Pagaduan, I. Barman, D. H. Gracias, *Angew. Chem. Int. Ed.* **2017**, *56*, 3822.
[34] A. M. Leferink, C. A. van Blitterswijk, L. Moroni, *Tissue Eng., Part B* **2016**, *22*, 265.
[35] G. A. Epling, C. Lin, *Chemosphere* **2002**, *46*, 561.
[36] W.-J. Li, C. T. Laurencin, E. J. Caterson, R. S. Tuan, F. K. Ko, *J. Biomed. Mater. Res.* **2002**, *60*, 613.
[37] Y. Geng, P. Dalhaimer, S. Cai, R. Tsai, M. Tewari, T. Minko, D. E. Discher, *Nat. Nanotechnol.* **2007**, *2*, 249.
[38] F. Q. Schafer, G. R. Buettner, *Free Radical Biol. Med.* **2001**, *30*, 1191.
[39] J. R. Casey, S. Grinstein, J. Orlowski, *Nat. Rev. Mol. Cell Biol.* **2010**, *11*, 50.
[40] P. Mitchell, *Nat. Biotechnol.* **2001**, *19*, 1013.
[41] P. Vesely, *Scanning* **2007**, *29*, 91.
[42] H. Yuan, C. G. Khoury, H. Hwang, C. M. Wilson, G. A. Grant, T. Vo-Dinh, *Nanotechnology* **2012**, *23*, 075102.
[43] B. Mir-Simon, J. Morla-Folch, P. Gisbert-Quilis, N. Pazos-Perez, H. Xie, N. G. Bastús, V. Puntes, R. A. Alvarez-Puebla, L. Guerrini, *J. Opt.* **2015**, *17*, 114012.